Quantum transport in molybdenum disulfide and germanane transistors

Chen, Qihong

Chapter 2. Two channels transport in MoS_2

Abstract

Two-dimensional MoS_2 has shown promising characteristics for application in electronic devices. In this chapter, we study the quantum transport properties of MoS_2 field effect transistors on h-BN substrates. The results consist of two parts. First, the electron mobility of MoS_2 is found to be significantly improved by encapsulation between top and bottom h-BN flakes. With greatly reduced contact resistance due to ionic liquid gating, the insulator to metal transition is observed. Second, for the MoS_2/h-BN structure without the top h-BN cap, superconductivity is induced at the top layer of the MoS_2 by ionic liquid gating as expected; surprisingly, the metallic bottom layers controlled by the back gate show Shubnikov-de Haas oscillation under perpendicular magnetic fields after the suppression of superconductivity. Hence, artificial electronic structures could be developed by controlling the interaction between the hetero-states at the top and bottom surfaces of a single few-layer MoS_2 flake. Variable electronic functionalities could be developed through the interaction between the different electronic states, similar to conventional van der Waals heterostructures that are prepared by stacking different two-dimensional (2D) materials, where novel electronic properties emerge from the realignment of dissimilar bands or tunneling through them.

Submitted as

"Electrically tunable coupling between hetero surface states in few-layer MoS_2"

Q.H. Chen, J.M. Lu, L. Liang, O. Zheliuk, A. Ali, P. Sheng and J.T. Ye

2.1 Introduction

In the modern electronic industry, silicon-based transistors are reaching their scaling limit below 5 nm in size. Exploration of novel device structures and new channel materials has therefore attracted growing interest. As a potential alternative to Si, MoS_2 exhibits larger band gaps and lower dielectric constants [1]. Because of its layered structure, MoS_2 can be easily thinned down to uniformly thin layers. Prototypes of few-layer and monolayer MoS_2 transistors have been reported, showing promising device operation characteristics for applications [2–4].

In order to meet the requirements for high-speed electronic devices, it is desirable to improve the electron mobility of MoS_2-based transistors. Suspended MoS_2 shows 2-10 times greater mobility enhancement compared to that supported by conventional oxide substrates [5], but is still lower than the expectation for high-speed electronic devices. In addition, the fabrication process for suspended MoS_2 is very complicated, which means it is not practically efficient. Alternatively, using hexagonal boron nitride (h-BN) as the substrates is an appealing approach to improve the performance of MoS_2 transistors. h-BN is thermally and chemically inert and electrically insulating. More importantly, the surface of h-BN is atomically flat and free of dangling bonds, and it has a lattice constant similar to that of MoS_2. As a result, when a thin MoS_2 flake is encapsulated between two h-BN flakes, the performance can be significantly improved; a Hall mobility of 34000 $cm^2V^{-1}s^{-1}$ has been reported [6,7].

On the other hand, improving the functional properties of gate control on the channel material is beneficial for reaching a high on/off ratio as well as low power consumption. Recently, ionic liquid has been increasingly used as gate media for replacing the traditional oxide gate dielectrics. This is known as the electrical double layer (EDL) technique. The biggest advantage of EDL is its ability to induce extremely large carrier density at the sample surface. New electronic states are observed in this regime that is not accessible with conventional solid gates. In two-dimensional (2D) transition metal dichalcogenides (TMDs), the field effect doping by ionic liquid induces high conductivity states for both electron and hole transport [8,9]. Remarkably, superconductivity is observed at the liquid/TMD interface in MoS_2 [10,11], $MoTe_2$ [12] and WS_2 [13], providing a playground for studying and controlling 2D superconductivity. Interesting superconducting properties in this system have been discovered, such as Ising pairing due to large effective Zeeman fields, which results from the broken inversion symmetry and strong spin-orbit coupling. As a result, the superconductivity is protected from very strong magnetic fields parallel to the *ab*-plane of MoS_2 [14–16].

It is predicted that for multilayer MoS_2 electrical double layer transistors (EDLTs), ionic gating confines the charge carriers mainly to the top-most layer, hence the superconductivity at the liquid/MoS_2 interface shows strictly 2D characteristics [14]. The top layer is well isolated electronically, acting like a free-standing monolayer, whereas the bottom layers (two layers away from the top) remain almost unaffected by ionic gating. It is expected that the top superconducting layer and bottom layers are electronically separated, forming two parallel conducting channels: a superconducting top channel and a normal bottom channel. The different electronic states at the top and bottom surfaces mimic the artificial van der Waals heterostructures stacked by different 2D materials, and new functionalities could be developed through their interaction. Nevertheless, no direct observation has been reported to corroborate this model of two conducting channels.

In this chapter, we first study the quantum transport properties of a MoS_2 transistor encapsulated between two h-BN flakes, with a partially exposed surface designed for electrical contacts. With the application of ionic gating, the exposed MoS_2 surface is turned into a metallic state by inducing a large carrier density, greatly improving the contact between the MoS_2 and electrodes. As a result, transport properties can be precisely measured at low temperatures, where the device shows improved carrier mobility. In addition, an insulator to metal transition controlled by the back gate is observed, suggesting that h-BN encapsulation suppresses the disordered potential so that the raised Fermi levels by the back gate can easily exceed the mobility edge.

In this device configuration, however, superconductivity cannot be induced because the ionic liquid and MoS_2 channel are separated by h-BN and the gating effect on the channel is very weak, ionic gating mainly helps with improving the contact. To overcome this difficulty and verify the two conducting channels model, we fabricated a MoS_2-EDLT on the h-BN substrate without a top h-BN capping flake. In this way, superconductivity can be easily induced at the liquid/MoS_2 interface, while high carrier mobility is maintained because of the atomically flat h-BN substrate. At low temperatures a sharp resistance drop from finite to zero resistance is observed, corresponding to the superconducting transition. After suppressing superconductivity in the out-of-plane magnetic field B, the parallel metallic state at the bottom surface of the MoS_2 is revealed by the observation of Shubnikov-de Haas (SdH) oscillation, which serves as direct evidence for the existence of a high mobility and low carrier density channel. The carrier density extracted from the oscillation of high-mobility electrons is found to be more than one order of magnitude smaller than that derived from the Hall effect, which includes carrier contributions from the whole flake, thus unambiguously confirming the formation of two spatially separated conducting channels.

2.2 Device fabrication

MoS_2 flakes were prepared by mechanical exfoliation of the 2H polytype bulk crystals (SPI supplies), using the well-known scotch tape method [17]. Silicon wafers coated with 300 nm-thick SiO_2 were used as substrates. Optical microscopy and atomic force microscopy (AFM) were used to identify the number of layers of MoS_2. h-BN flakes were prepared on different silicon wafers in a similar way. Uniformly thin MoS_2 flakes in the range of 1-5 layers and h-BN flakes with thicknesses of 10-30 nm were selected for device fabrication.

After preparing MoS_2 and h-BN flakes on separate Si/SiO_2 substrates, we use the so-called dry transfer technique [18,19] to fabricate the van der Waals heterostructure. The transfer process is illustrated schematically in Figure 2.1, which shows an example of making the h-BN/MoS_2/h-BN heterostructure. A thin film of polycarbonate (PC) is prepared by first dissolving the PC pellets in chloroform and putting a few droplets of the solution onto a cover glass. Another cover glass is put on top to spread out the solution, and then the two cover glasses are separated by sliding them over each other. After a few minutes, the chloroform solvent evaporates and a thin uniform PC film is left on the glass. The PC film is then carefully removed from the glass substrate and fixed on top of a piece of polydimethylsiloxane (PDMS) on a thin glass slide with dimensions of ~3×3×1 mm. The cover glass with the PDMS and PC film used as a stamp to pick up MoS_2 and h-BN flakes; it is inverted and fixed on a micro-manipulator with xyz-movement. The stamp is gradually brought into contact with the SiO_2/Si substrate until the PC film almost touches the target h-BN flake. Then the SiO_2/Si substrate with h-BN is heated to about 90 °C, allowing the real contact of PC film and h-BN due to thermal expansion. After that, the heating is stopped and the stamp gradually retracts from the substrate. Because the adhesion between the h-BN and PC film is stronger than that between the h-BN and substrate, the h-BN flake is picked up by the PC film. The whole structure (h-BN + PC + PDMS) is used as a stamp to pick up the target MoS_2 flake in a similar way, and this process can be repeated to pick up other crystals to form the desired stacking of different 2D materials.

After all the target flakes are picked up, the whole stamp with the stacked heterostructure is put in contact with the target substrate and heated up to 170 °C to melt the PC film. The stamp is carefully retracted, leaving the PC film as well as the stacked structure on the substrate. The PC film on top of the heterostructure can be removed by dissolving it in chloroform. The flakes are not exposed to any solvent until the whole heterostructure is completed; the interface remains relatively clean, which is important for achieving high carrier mobility. Then reactive ion etching (RIE) is used to shape the sample into Hall bar geometry, and metal contacts are made by the standard electron beam lithography procedure.

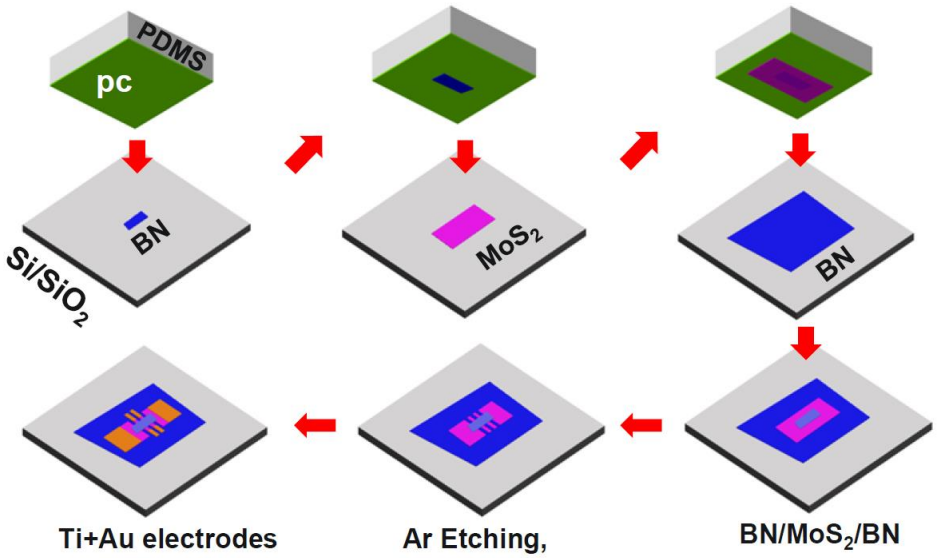

Figure 2.1 Dry transfer process for preparing the h-BN/MoS_2/h-BN heterostructure. The top h-BN flake is carefully chosen so that it covers the MoS_2 surface only partially; the exposed area is used for contact electrodes as well as ionic gating. Sandwiched MoS_2 is etched into Hall-bar geometry with RIE etching, and Ti/Au electrodes are patterned using standard electron beam lithography. The process can be modified to fabricate any other desired device structures, such as MoS_2/h-BN or MoS_2 transistors on an HfO_2 substrate.

2.3 Results and discussions

In the following, we focus on the measurement results of two device configurations. The first is a MoS_2 transistor encapsulated between top and bottom h-BN flakes. For ionic gating, the MoS_2 conducting channel and liquid is separated by h-BN; only the exposed area for contact electrodes is heavily doped by ionic gating. The second is a MoS_2-EDLT device on an h-BN substrate, without any h-BN capping on top. The whole MoS_2 surface can be gated by ionic liquid and becomes superconducting at low temperatures. The bottom layers stay semiconducting which can be tuned by the back gate as a conventional transistor.

2.3.1 MoS_2 encapsulated between top and bottom h-BN

Figure 2.2(a) shows the optical image of an h-BN/MoS_2/h-BN heterostructure on SiO_2/Si substrate. A few-layer MoS_2 flake is sandwiched between two h-BN flakes, with a partially exposed surface designed for metal contacts. Figure 2.2(b) shows the transfer curve at different temperatures before applying ionic gating. The device can be switched on and off by the back gate, showing an n-type

transistor operation with a current on/off ratio higher than 10^2. However, a clear decrease of the source-drain current is observed as the temperature decreases, which is most likely associated with the increase in contact resistance. It is well known that because of the work function difference between metal electrodes and semiconducting MoS_2, there is a potential barrier for electrons, namely the Schottky barrier. For a fixed source-drain voltage, the temperature dependence of the current is given by $I = A^* T^2 e^{-\frac{q\Phi_b}{kT}}(e^{\frac{qV}{kT}} - 1)$, where A^* is a constant and q and k are the electron charge and Boltzmann constant, respectively. V is the source-drain voltage and Φ_b is the height of the barrier. From this relation we see that the source-drain current decreases when the temperature decreases, in line with our observation.

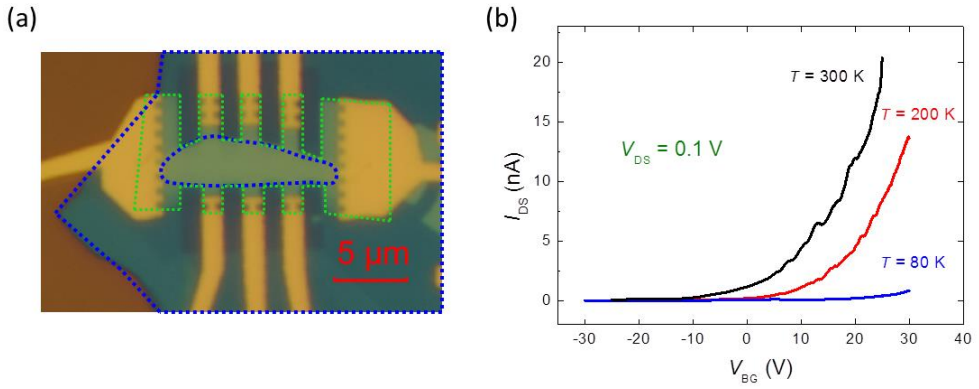

Figure 2.2 (a) Optical image of a typical h-BN/MoS_2/h-BN device. Top h-BN is highlighted by the blue dashed line in the center. The green dashed line depicts the edge of the MoS_2, and the large dark area surrounded by the blue dashed line is the bottom h-BN flake. The top h-BN is smaller than the MoS_2 flake, metal contacts are made in the exposed area. Electrodes are composed of 5 nm Ti / 65 nm Au. (b) Transfer curves of transistor operations by the SiO_2 back gate at different temperatures, with fixed source-drain voltage V_{DS} = 0.1 V. An n-type transistor operation is observed with source-drain current on/off ratio ~ 10^2.

As mentioned above, the contact resistance can be greatly reduced by applying ionic liquid gating. Figure 2.3(a) shows a schematic of the gating configuration. When a positive voltage is applied between the gate pad and the MoS_2 flake, cations are driven very close to the surface of the exposed MoS_2, forming a nanogap capacitor with very large capacitance. The induced carrier density is in the order of ~10^{14} cm^{-2}; hence the Fermi level can be significantly altered by ionic gating. According to the phase diagram [10,20], the insulator-metal transition occurs at 8×10^{12} cm^{-2} for multilayer MoS_2. As a result, the exposed MoS_2 surface

behaves like a normal metal, and the contact resistance is significantly reduced locally at the exposed area.

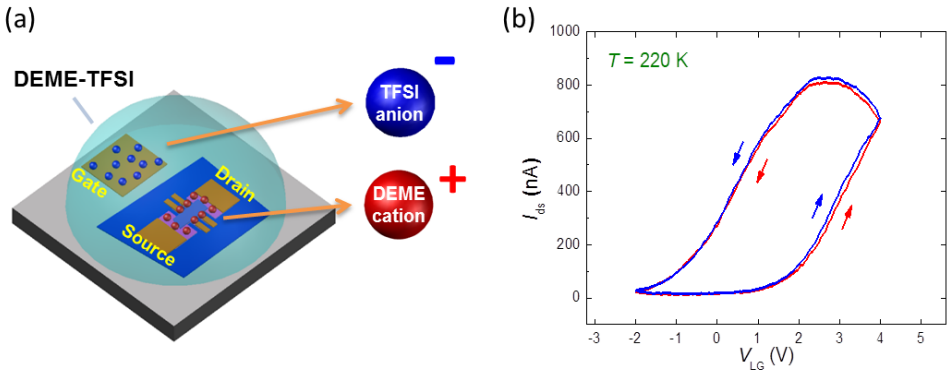

Figure 2.3 (a) Schematics of the MoS_2-EDLT device and measurement configuration. With positive liquid gate voltage, cations are driven very close to the exposed surface of the MoS_2 and induce a lot of electrons in these local areas. (b) Transfer curves of transistor operations by the liquid gate at T = 220 K, for the same device as shown in Figure 2.2, showing a remarkable enhancement of gating effect compared with the SiO_2 solid gate.

The transfer curves by liquid gating are shown in Figure 2.3(b), where the arrows indicate the gate voltage sweeping direction. To retain the high mobility of cations/anions as well as protect the sample from the electrochemical reaction, the ionic gating procedure is conducted at T = 220 K, as has been well established in previous studies [9–14,21,22]. The device can also be switched on and off with ionic gating, and the required voltage is much lower compared to that of the SiO_2 back gate, suggesting that the efficiency of the liquid gate is much higher than that of the solid gate. The source-drain current is nearly two orders of magnitude higher than SiO_2 back gating at T = 200 K, showing a great improvement in the FET performance. We also see that the first cycle (red) and the second cycle (blue) almost coincide with each other, indicating that no chemical reaction happens during the gating procedure, which means the doping is electrostatic. However, a large hysteresis is observed due to the low ion mobility at relatively low temperatures. This is the disadvantage of gating at low temperatures, and the uniformity of the gating will also be affected.

We cooled the device down to liquid nitrogen temperature to measure the temperature dependence of the MoS_2 channel resistance. Normally the gate voltage is retained before it is cooled down to freeze the ion movement. Once the temperature is below the freezing point of the ionic liquid, ions cannot move, and the gate voltage can be retracted without losing the gating effect. As shown in Figure 2.4(a), the two black curves represent the temperature dependence of the

channel resistance before applying ionic gating. If the back gate voltage is zero, which means that the MoS_2 channel is not gated, it behaves as an intrinsic insulator with very high resistance (top black curve with label V_{BG} = 0 V, V_{LG} = 0 V). With applied back gate voltage V_{BG} = 60 V, the MoS_2 channel shows a metallic behavior at T > 120 K, where the resistance decrease as the temperature goes down. With further cooling down to below 120 K, sample resistance starts to increase. We did not perform the Hall measurement on this device because it was measured in a setup that is not equipped with magnet. Therefore the carrier density cannot be determined accurately. Alternatively, because the carriers are induced by back gate, the corresponding carrier density can be estimated from the geometric capacitance of back gate through $n_{2D} = C_g(V_{BG} - V_{th})/e$, where V_{BG} is the applied back gate voltage; e is the charge of electron; $C_g = 10.5$ nF/cm^2, which is the capacitance per unit area considering the back gate of 300 nm SiO_2 and 30 nm h-BN used in this experiment; and V_{th} = 40 V, which is the threshold voltage that can be extracted from the transfer curve, as shown in Figure 2.4(b) (black curve with V_{LG} = 0 V). Therefore, the induced 2D carrier density is n_{2D} = 1.3×10^{12} cm^{-2}. This relatively low carrier density with metallic behavior proves that the quality of the sample device is good.

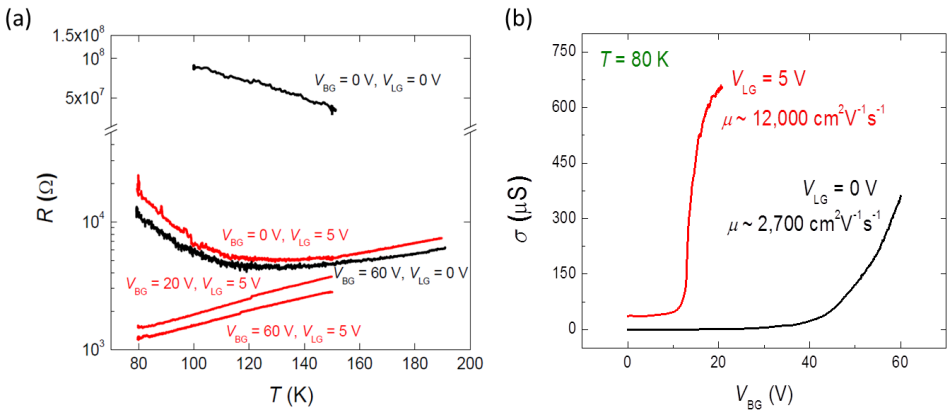

Figure 2.4 (a) Comparison of the temperature dependence of the channel resistance before (black curves) and after (red curves) applying ionic gating. With the application of ionic gating V_{LG} = 5 V, channel resistance undergoes a transition from insulating behavior (V_{BG} = 0 V) to metallic behavior (V_{BG} = 20 V). (b) Transfer curve with SiO_2 back gate at low temperatures (T = 80 K). Mobility extracted from the gate dependence of conductivity is 2700 cm^{2}V^{-1}s^{-1} before and 12000 cm^{2}V^{-1}s^{-1} after applying ionic gating, showing great enhancement.

The red curves in Figure 2.4(a) show the temperature dependence of the MoS_2 channel resistance under different back gate voltages, with the ionic gate voltage

fixed at V_{LG} = 5 V. A different behavior is observed comparing to before applying ionic gating. For V_{LG} = 5 V and V_{BG} = 0 V, the RT curve is very similar to that of V_{LG} = 0 V and V_{BG} = 60 V. This result implies that even though there is a top h-BN flake covering the MoS_2 conducting channel, ions can still accumulate at the top surface of the h-BN and induce carriers in the MoS_2 channel. With a 20 nm-thick h-BN flake in this device, the induced carrier is similar to that of the 60 V back gate. For V_{LG} = 5 V and V_{BG} = 20 V, the sample shows metallic behavior ($dR/dT > 0$) until the liquid nitrogen temperature, and becomes more conducting at the higher back gate V_{BG} = 60 V.

Figure 2.4 (b) shows the conductivity as a function of back gate voltage, before (black curve) and after (red curve) applying the liquid gate. The threshold voltage shifts to the left side due to the weak doping effect by the ionic gating through the h-BN, and for V_{LG} = 5 V the conductivity increases much faster than V_{LG} = 0 V, corresponding to a higher mobility. The FET mobility can be estimated by the back gate dependence of conductivity through $\mu_{FET} = \frac{1}{C_g}\frac{d\sigma}{dV_{BG}}$, where σ is the conductivity and C_g is the gate capacitance per unit area. Here, for 300 nm SiO_2 and 30 nm h-BN $C_g = 10.5\ nF/cm^2$. We can estimate the mobility from the linear fitting in the vicinity of threshold voltage. Before and after applying the ionic gating, the extracted mobilities are 2700 and 12000 $cm^2V^{-1}s^{-1}$, respectively. The enhancement of mobility may be related to the fact that there is ion accumulation at the surface of the top h-BN, these ions form a charge screening layer which helps to reduce the scattering from the charged impurities in the MoS_2 channel. Hence the mobility increases. It should be noted that the off-state current for V_{LG} = 5 V is higher than that of V_{LG} = 0 V. While this may be due to the gating effect of the MoS_2 channel edge, further investigation is needed to study this behavior.

2.3.2 MoS_2-EDLT on h-BN substrate without top cover

With MoS_2 covered by a top h-BN, ionic gating is able to induce carriers in the MoS_2 channel. However, the carrier density is not high enough to reach superconducting state. To prove the two parallel conducting channels that form due to the dual-gate configuration, we modified the device structure by removing the top capping h-BN flake. With the application of ionic gating in this configuration, the top surface of the MoS_2 becomes highly doped, whereas the bottom layers remain almost unaffected. The high electron mobility nature of the bottom layers is preserved due to the atomically flat bottom h-BN substrate. Novel electronic functionalities emerge through the interplay of the superconducting top surface and high mobility bottom surface. The device structure is similar to that of high electron mobility transistors (HEMTs), which are conventionally fabricated

with semiconducting planar junctions with different band structures, such as GaAs and AlGaAs, using a molecular beam evaporation technique [23].

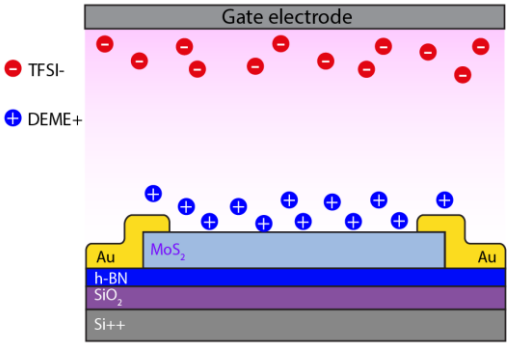

Figure 2.5 Dual-gate device configuration of MoS_2/h-BN transistor on SiO_2/Si++ substrate. Without top h-BN cover, the MoS_2 surface is in contact with the ionic liquid; thus the whole surface becomes highly doped by ionic gating.

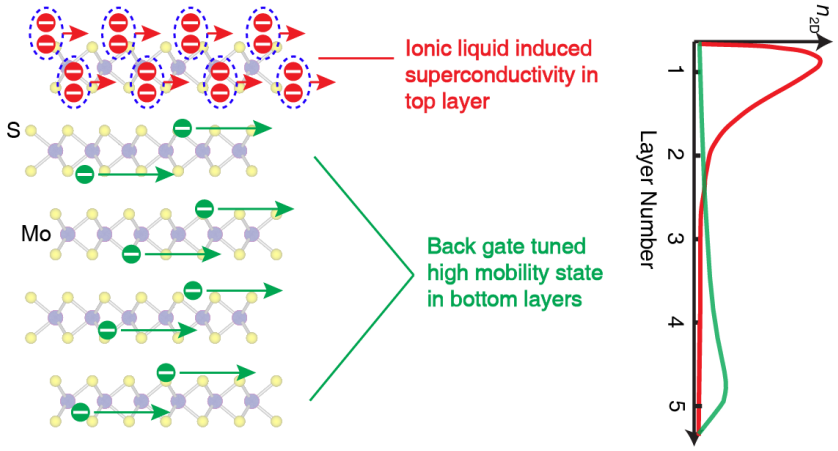

Figure 2.6 Illustration of the doping profile by the ionic liquid gate and solid-state back gate. The layer number is labeled as "1" for the topmost layer and "5" for the bottommost layer. Due to the strong Thomas-Fermi screening effect, the doping effect from ionic gating decays exponentially for individual layers from top to bottom. The back gating effect also decays from bottom to top, but it is much slower because the carrier density induced by the back gate is much smaller.

The schematic device configuration of the MoS_2-EDLT device on the h-BN substrate is shown in Figure 2.5. Since the top surface of the MoS_2 is not covered by h-BN, superconductivity can be easily induced by ionic gating. Theoretical calculations show that with 2D carrier density n_{2D} of the topmost surface induced

by ionic gating in the order of ~10^{14} cm^{-2}, the number of accumulated carriers for individual layers decays exponentially from the top to bottom due to the strong Thomas-Fermi screening effect [24]. The n_{2D} of the second layer is reduced by almost 90% compared to that of the first one. Therefore, the superconducting topmost layer is well isolated electronically from the rest of the layers below and acts like a freestanding monolayer [25]. The bottom layers remain almost undoped. On the other hand, the back gate mainly induces carriers in the bottom layers. The electron mobility in the bottom layers on h-BN is very high, suitable for making HEMTs. The rough carrier density profile is shown in Figure 2.6, where the layer number "1" denotes the topmost layer and "5" denotes the bottommost layer. The screening effect is inversely scaled with the carrier density; the ionic gating induces large carrier density but decays abruptly from top to bottom, while the back gating induces smaller carrier density but tends to influence more layers.

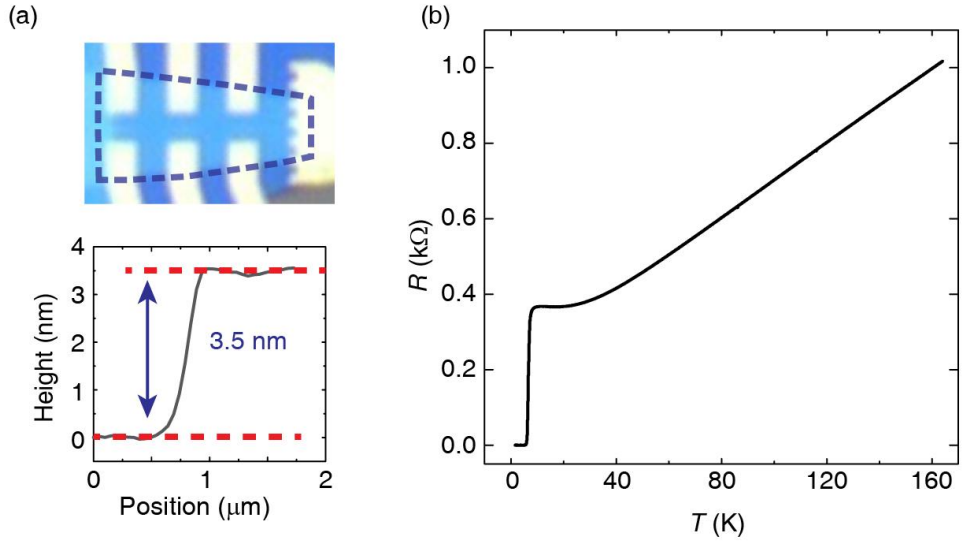

Figure 2.7 (a) Top panel: optical image of a MoS_2-EDLT device on an h-BN substrate, with MoS_2 highlighted by the dashed line. Bottom panel: AFM height profile of the MoS_2 flake, showing that the thickness of the MoS_2 in this study is 3.5 nm, corresponding to a layer number of five. (b) Temperature dependence of the channel resistance with fixed ionic liquid gate voltage V_{LG} = 6 V.

For ionic gating, all the conditions are kept the same as detailed in the previous section. Figure 2.7(a) shows the optical image (top panel) and the AFM height profile (bottom panel) of the measured device. For a layered material with layer number N, the corresponding thickness is $d = a + (N-1) \times b$, where a is the height of the bottom layer (including the space between the bottom layer and the

substrate) and b is the layer thickness. In MoS_2, the typical value of a ranges from 0.8 to 1 nm depending on the adhesion between the flake and the underlying substrates, while b is around 0.62 nm [26,27]. The thickness of the studied MoS_2 flake is 3.5 nm characterized by AFM (Figure 2.7(a), bottom panel), and consequently the number of layers is five. The ionic gate voltage V_{LG} was applied at T = 220 K, and then the sample was cooled down to measure the temperature dependence of channel resistance. The channel resistance decreases as the temperature decreases, showing metallic behavior. The RT curve becomes flat below T = 30 K, which is likely due to the impurity scatterings and doping inhomogeneity. A sharp resistance drop is observed below T = 10 K, corresponding to the superconducting transition with T_c = 7 K. The transition temperature T_c is defined as 50% of the normal state resistance. Zero resistance is observed with further cooling down.

The RT behavior is different with different ionic gate voltages, as shown in Figure 2.8. For V_{LG} = 3 V, the sample shows metallic behavior, but no superconductivity is observed until T = 2 K, this state is very close to the quantum critical point (QCP). With increasing liquid gate voltage, superconductivity starts to appear. T_c shifts to higher temperatures for higher gate voltages with a tendency to saturate at V_{LG} > 4.6 V.

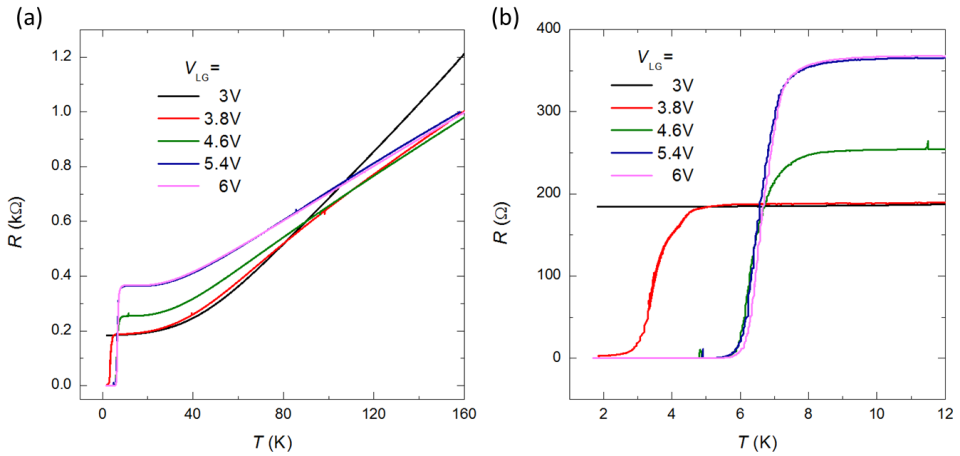

Figure 2.8 (a) Temperature dependence of MoS_2 channel resistance for different ionic gate voltages. (b) Low temperature region of the same data set as in Figure 4-7(a).

At low temperatures, we measured the temperature dependence of resistance under different magnetic fields, which were applied perpendicularly to the surface of the MoS_2. Figure 2.9 shows the results for liquid gate voltage V_{LG} = 4.6 V. The superconducting transition is dramatically suppressed by the magnetic field.

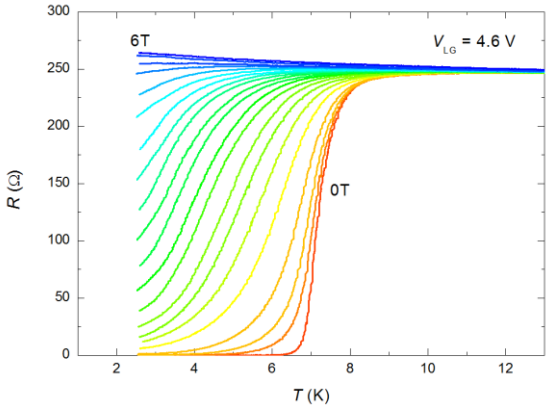

Figure 2.9 Sheet resistance of the MoS_2-EDLT device as a function of temperature for V_{LG} = 4.6 V under perpendicular magnetic fields, 0, 0.05, 0.1T, 0.2 to 2.4 T in 0.2 T steps, 2.7, 3, 3.5, 4, 5 and 6 T. Superconductivity is gradually suppressed by the magnetic field.

Without applying back gate voltage, the bottom layers remain insulating and make no contribution to the conductivity of the MoS_2 channel. Superconductivity originates solely from the top layer, which has a high carrier density (~10^{14} cm^{-2}). With positive back gate voltage applied, electrons start to accumulate at the bottom layers. As a result, the conductivity of the bottom layers increases and two parallel conducting channels form in a single few-layer MoS_2 flake.

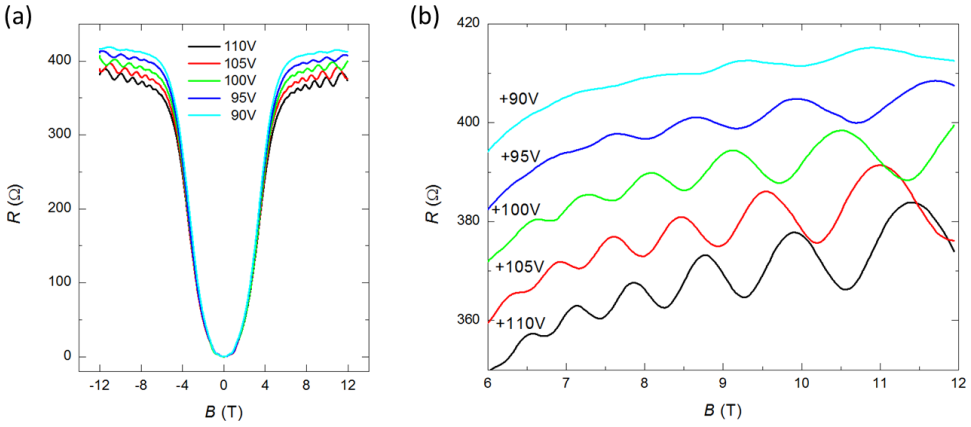

Figure 2.10 (a) Longitudinal resistance as a function of the magnetic field measured at T = 2 K and V_{LG} = 6 V, for back gate voltages from 90 to 110 V in 5 V steps. (b) Magnified view of the region between 6 and 12 T.

Figure 2.10 shows the longitudinal magnetoresistance (MR) for different V_{BG} values at T = 2 K and V_{LG} = 6 V. Without the magnetic field, the MoS_2 is in a

superconducting state, and resistance is zero. When the applied magnetic field increases, the resistance also increases as expected due to the suppression of superconductivity. Surprisingly, pronounced Shubnikov-de Haas (SdH) oscillations are observed after the superconductivity is suppressed by the magnetic field. As the back gate voltage increases from 90 to 110 V, the amplitude of the oscillation becomes notably larger, due to the enhanced conductivity of the bottom layers. The peak and valley positions also change with different back gate voltages. In contrast, all the curves almost coincide with each other at the low field region, which suggests that the superconducting properties are not affected by the back gate. This can also be verified from the doping profile in Figure 2.6; the influence of the back gate on the superconducting layer is negligible due to the screening effect.

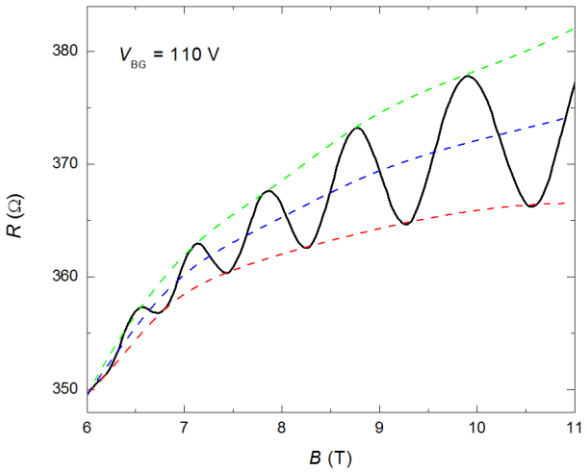

Figure 2.11 Determination of the magnetoresistance background for back gate voltage V_{BG} = 110 V. The green and red dashed lines denote the top and bottom envelop which are determined by the peaks and valleys of the oscillation, respectively. The average of the top and bottom envelope (blue dashed line) is taken as the magnetoresistance background for extracting the oscillation component.

According to theory, SdH quantum oscillations are a periodic function of the inverse of the magnetic field $1/B$. To carefully examine the oscillation behavior, we first subtract the MR background. As shown in Figure 2.11, the top (green dashed line) and bottom (red dashed line) envelope lines are determined by the peaks and valleys of the oscillations, respectively. The blue dashed line is the average of the top and bottom envelope lines and is taken as the MR background for extracting the oscillation component.

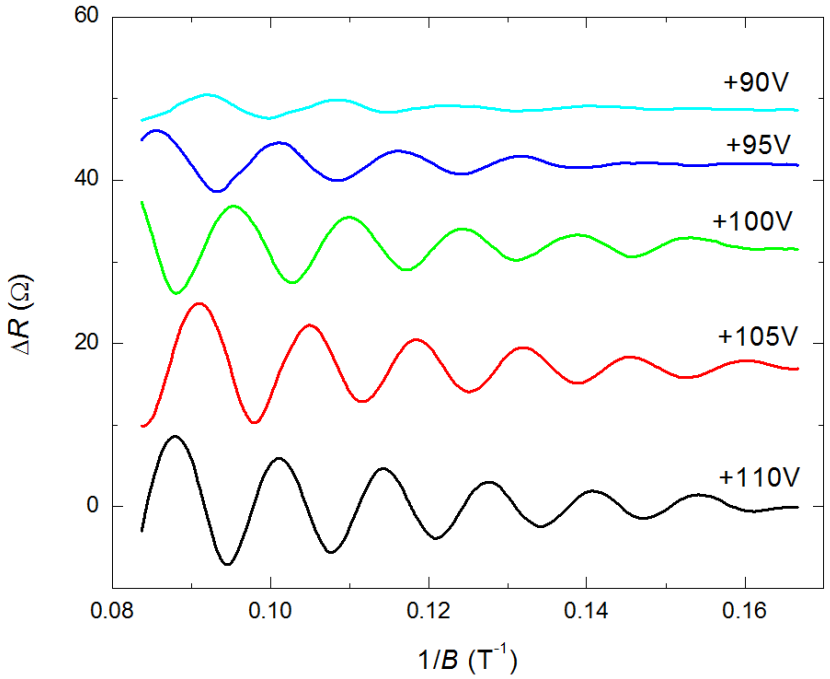

Figure 2.12 Oscillation amplitudes as a function of $1/B$ after subtracting the MR background for different back gate voltages corresponding to the same data set as shown in Figure 2.10. Curves are vertically shifted for clarity.

After subtracting the MR background and plotting as a function of the inverse of the magnetic field $1/B$, we see a clearly periodic oscillation and the oscillation period decreases with the increasing back gate voltage, as shown in Figure 2.12. According to theory, the envelope function of the oscillation in longitudinal resistance can be described by the Ando formula [28,29]:

$$\Delta R = 4R_0 e^{-\alpha T_D} \alpha T / \sinh(\alpha T)$$

Where R_0 is the classical resistance in zero applied field, $= 2\pi^2 k_B/\hbar\omega_c$, $\omega_c = eB/m^*$ is the cyclotron frequency and m^* is the electron effective mass. $\hbar$ is the reduced Planck constant, k_B is the Boltzmann constant. $T_D = \hbar/2\pi k_B\tau$ is the Dingle temperature and τ is the scattering time. For 2D electron gas, the carrier density n_{2D} is related to the period of the quantum oscillations through $n_{2D} = geB_F/h$, where g is the Landau level degeneracy and B_F is the oscillation frequency in $1/B$ which can be obtained from Figure 2.12. On the other hand, it is clear that the oscillation behavior is well controlled by back gate, hence n_{2D} can be obtained from the gate capacitance $n_{2D} = C_g(V_{BG} - V_{th})/e$. Here V_{th} is the threshold voltage

and $C_g = 10.5$ nF/cm^2 is the capacitance per unit area for the back gate of 300 nm SiO_2 and 30 nm h-BN used in this experiment. Thus, we have

$$B_F = \frac{hC_g}{ge^2}(V_{BG} - V_{th})$$

Hence Landau level degeneracy g can be obtained from the linear fitting of the back gate dependence of B_F, as shown in Figure 2.13. The result shows that g = 3.16, consistent with that of the previous report [7].

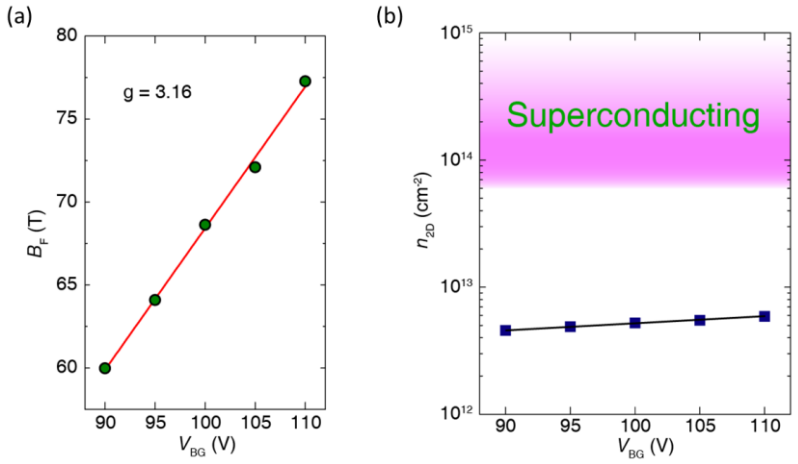

Figure 2.13 (a) Oscillation period B_F as a function of back gate voltage obtained from the period of oscillation. The linear fitting yields a Landau level degeneracy of 3.16. (b) The density of carriers that accounts for the quantum oscillations at different back gate voltages (solid dots connected by black line), extracted from the oscillation period. Shaded area indicates the carrier densities where MoS_2 is superconducting, the bottom of this area represents the quantum critical point (QCP) of the superconducting phase diagram.

With the obtained Landau level degeneracy, we are able to estimate the density of carriers that accounts for the SdH oscillations through $n_{2D} = geB_F/h$. The results are shown in Figure 2.13(b). For all V_{BG}, the carrier densities that accumulate at the bottom surface are more than one order of magnitude lower than the lowest value for reaching superconductivity (~6×10^{13} cm^{-2}). This unambiguously confirms the existence of two conducting channels with high and low carrier densities responsible for superconductivity and SdH oscillation, respectively. This is exactly what was expected: ionic gating confines carriers to the topmost layer, which becomes superconducting, while bottom layers remain intrinsically semiconducting. With a positive back gate, the bottom channel becomes electron doped and conducting. The electron mobility in the bottom channel is very high due to the atomically flat h-BN substrate, and SdH oscillations are contributed by this channel. SdH oscillations in MoS_2 have been observed in

previous reports, either when graphene was used as contacts [6] or when MoS_2 was encapsulated between the top and bottom h-BN [7]. In our case, the MoS_2 flake was not covered with a top h-BN; the top superconducting layer of MoS_2 itself becomes a piece of normal metal after the superconductivity is suppressed by the magnetic field, acting as a screening layer that functions the same as or even better than a top protecting h-BN. Furthermore, the induced superconducting top channel (metallic at the high magnetic fields) serves as a metallic contact for the encapsulated bottom layers that ensures the observation of SdH oscillations. These advantages make the fabrication process very simple.

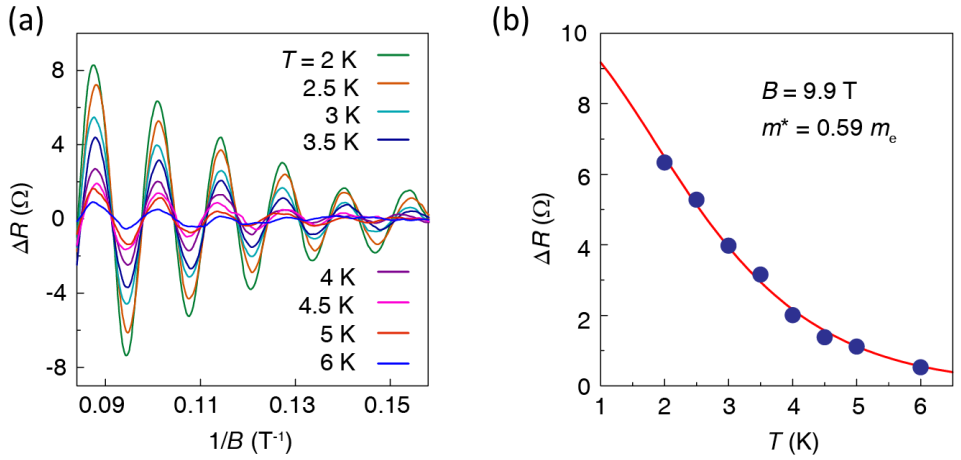

Figure 2.14 (a) ΔR as a function of $1/B$ measured at different temperatures from 2 to 6 K, for V_{BG} = 110 V. The oscillation is gradually suppressed with increased temperature and almost disappears at T = 6 K, owing to the enhanced electron-phonon scattering. (b) Solid dots show the temperature dependence of the oscillation amplitude at B = 9.9 T. By using the Ando formula $\Delta R \propto \alpha T/\sinh(\alpha T)$, the best fitting (red curve) gives an electron effective mass of 0.59 m_e. Fittings at other magnetic fields are not shown here but give similar and consistent results.

Figure 2.14(a) shows the temperature dependence of the SdH oscillation amplitudes at V_{BG} = 110 V. With increased temperatures, the quantum oscillations are gradually suppressed due to the enhanced electron-phonon scattering. The effective mass of the conducting electron can be deduced by fitting the temperature-dependent oscillation amplitudes with the Ando formula at a fixed magnetic field. With the amplitude proportional to $\Delta R \propto \alpha T / \sinh(\alpha T)$, as shown in Figure 2.14 for B = 9.9 T, the best fitting yields an effective mass of m^* = 0.59 m_e, where m_e is the bare electron mass. In theoretical calculations of the MoS_2 band structure there are two bands near the Fermi level (K and Q), while the lowest energy is at the K valley (m^* = 0.5 m_e) for monolayer MoS_2, the Q valley (m^* = 0.6 m_e) becomes the lowest for layer number greater than 2L [6,30]. Since the

MoS_2 flake in this study is five layers, the result is in excellent agreement with the theoretical value.

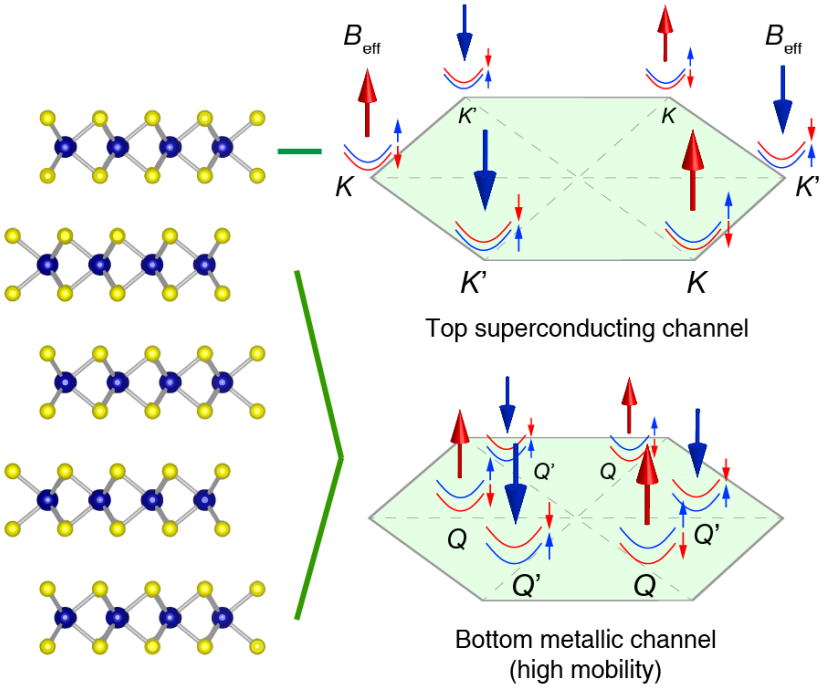

Figure 2.15 Conduction band edge corresponding to the Brillouin zone of the top and bottom channels, where blue and red represent the spin-up and spin-down bands, respectively. For the top superconducting channel, the minima of the conduction band reside at the *K*/*K'* valleys; whereas for the bottom high mobility channel, the conduction band minima are at the *Q*/*Q'* valleys which sit in between the Γ and *K*/*K'* points. The large red and blue arrows indicate the effective Zeeman fields that cause the spin splitting, which is opposite for the *K(Q)* and *K'(Q')* points.

To summarize, the electronic states of two channels are shown schematically in Figure 2.15. The top-most layer is highly doped and well isolated electronically [14,15], which behaves like a monolayer, with the lowest energy of the conduction band located at the *K*/*K'* valleys, whereas for the rest of the flake the lowest energy of the conduction band is at the *Q*/*Q'* valleys. Spin degeneracies in each *Q* and *Q'* valleys are lifted by the intrinsic Zeeman field B_{eff}, which accordingly aligns spin in opposite directions at the *Q* and *Q'* valleys of the Brillouin zone. The degeneracy 6 composed of 3*Q* and 3*Q'* valleys is further removed by the valley Zeeman effect with an applied external magnetic field [7,31]. Thus the Landau level degeneracy *g* equals 3, which is consistent with the $g = 3.16$ observed experimentally.

An unusual behavior is observed in the transition temperature T_c of the top superconducting channel, as shown in Figure 2.16. As the back gate voltage increases, T_c first increases and then decreases. According to the phase diagram, the positive back gate accumulates electrons in the MoS_2 channel, which in principle leads to the increase in T_c. The unusual decrease in T_c suggests that due to the growing conductivity of the bottom channel, enhanced interaction with the top surface plays an important role in determining superconducting properties. This behavior will be discussed in more detail in the next chapter.

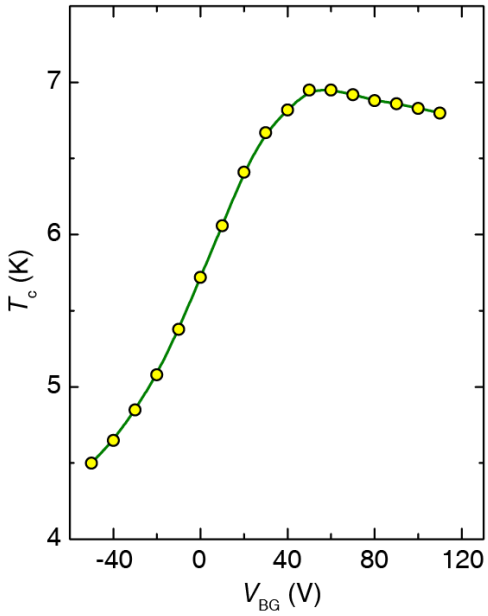

Figure 2.16 Superconducting transition temperature T_c as a function of applied back gate voltage, for V_{LG} = 6 V. As back gate voltage increases, T_c first increases and then decreases, which is not consistent with the phase diagram.

As a summary, Figure 2.17 plots the magnetoresistance of the MoS_2 device for different applied ionic gate voltages at the lowest temperature T = 2 K, with fixed back gate voltage V_{BG} = 100 V. The oscillations become more evident as the ionic gate voltage increases, because higher ionic voltage induces higher carrier density at the top surface, which leads to a stronger screening effect, so the bottom layers are better protected from the environment. The peak and valley positions of the oscillation remain almost unchanged, indicating that the band structure of the bottom layers is not affected by the top ionic gating, consistent with the band edge of the two parallel channels as shown in Figure 2.16.

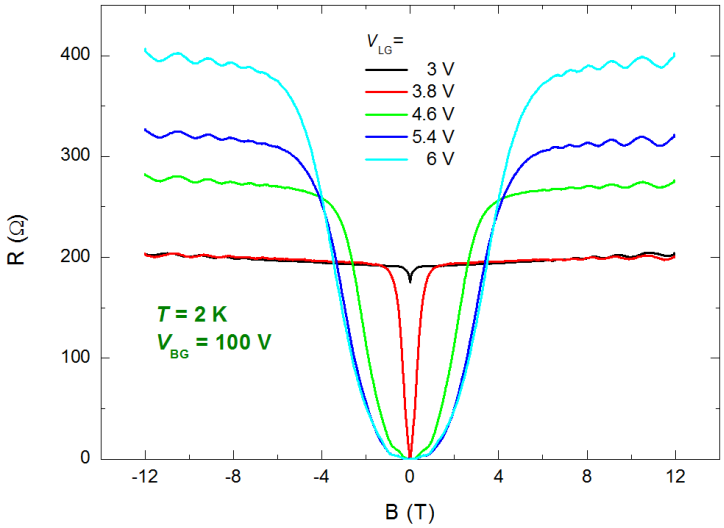

Figure 2.17 Magnetoresistance of MoS_2 for different ionic gate voltages, with fixed back gate V_{BG} = 100 V, at T = 2 K. The peak and valley positions of the oscillations remain almost the same.

2.4 Conclusion

This chapter studied the quantum transport of two types of MoS_2 transistor devices:

(1) MoS_2 encapsulated between two h-BN flakes. With protection from top and bottom h-BN flakes, high electron mobility reveals the high quality and homogeneity of our MoS_2 transistors. The insulator to metal transition is observed at relatively low carrier density, providing additional evidence for the good quality of the heterostructure. Ionic liquid gating is found to improve device performance by greatly reducing the contact resistance. Surprisingly, although ionic liquid and MoS_2 surface are separated by a 20 nm-thick h-BN flake, ions can still accumulate at the surface of the h-BN. These ions act as a screening layer which further improves the electron mobility of the MoS_2 channel.

(2) MoS_2 FET without a top h-BN flake. The top surface of the MoS_2 channel can be directly gated by ionic liquid and becomes superconducting at low temperatures. Clear SdH quantum oscillations are observed in the magnetoresistance after the superconductivity is suppressed by the magnetic field. The carrier density is more than one order of magnitude lower than the value derived from the Hall measurements, which unambiguously confirms the existence of two parallel conducting channels in few-layer MoS_2-EDLT devices.

Superconductivity is induced at the top surface of the MoS_2 by ionic gating; the induced carrier is in the order of ~10^{14} cm^{-2}. Due to the strong screening effect of the large carrier density, the bottom layers remain unaffected by the ionic gating, and the conductivity of the bottom layers can be continuously controlled by the back gate as a conventional field effect transistor. Therefore, two parallel conducting channels form at the top and bottom surfaces of the MoS_2, accounting for the superconductivity and SdH quantum oscillation, respectively. The superconducting channel acts as a screening layer as well as metal contact for probing SdH oscillations under a high magnetic field when superconductivity is suppressed. Furthermore, the effective mass and Landau level degeneracy extracted from the oscillation amplitude are in excellent agreement with theoretical calculations. This is the first experimental observation that firmly confirms the coexistence of two parallel conducting channels in a single MoS_2 flake.

References

[1] S.B. Desai, S.R. Madhvapathy, A.B. Sachid, J.P. Llinas, Q. Wang, G.H. Ahn, G. Pitner, M.J. Kim, J. Bokor, C. Hu, H.-S.P. Wong, A. Javey, MoS_2 transistors with 1-nanometer gate lengths, *Science.* 354 (2016) 99–102.

[2] K.S. Novoselov, D. Jiang, F. Schedin, T.J. Booth, V.V. Khotkevich, S.V. Morozov, A.K. Geim, Two-dimensional atomic crystals, *Proc. Natl. Acad. Sci.* U. S. A. 102 (2005) 10451–10453.

[3] A. Ayari, E. Cobas, O. Ogundadegbe, M.S. Fuhrer, Realization and electrical characterization of ultrathin crystals of layered transition-metal dichalcogenides, *J. Appl. Phys.* 101 (2007) 14507.

[4] B. Radisavljevic, A. Radenovic, J. Brivio, V. Giacometti, A. Kis, Single-layer MoS_2 transistors, *Nat. Nanotechnol.* 6 (2011) 147–150.

[5] T. Jin, J. Kang, E.S. Kim, S. Lee, C. Lee, Suspended single-layer MoS_2 devices, *J. Appl. Phys.* 114 (2013) 164509.

[6] X. Cui, G.-H. Lee, Y.D. Kim, G. Arefe, P.Y. Huang, C.-H. Lee, D.A. Chenet, X. Zhang, L. Wang, F. Ye, F. Pizzocchero, B.S. Jessen, K. Watanabe, T. Taniguchi, D.A. Muller, T. Low, P. Kim, J. Hone, Multi-terminal transport measurements of MoS_2 using a van der Waals heterostructure device platform, *Nat. Nanotechnol.* 10 (2015) 534–540.

[7] Z. Wu, S. Xu, H. Lu, G.-B. Liu, A. Khamoshi, T. Han, Y. Wu, J. Lin, G. Long, Y. He, Y. Cai, F. Zhang, N. Wang, Observation of Valley Zeeman and Quantum Hall Effects at Q Valley of Few-Layer Transition Metal Disulfides, *ArXiv*151100077 Cond-Mat. (2015).

[8] Y. Zhang, J. Ye, Y. Matsuhashi, Y. Iwasa, Ambipolar MoS_2 Thin Flake Transistors, *Nano Lett.* 12 (2012) 1136–1140.

[9] Y.J. Zhang, J.T. Ye, Y. Yomogida, T. Takenobu, Y. Iwasa, Formation of a Stable p–n Junction in a Liquid-Gated MoS_2 Ambipolar Transistor, *Nano Lett.* 13 (2013) 3023–3028.

[10] J.T. Ye, Y.J. Zhang, R. Akashi, M.S. Bahramy, R. Arita, Y. Iwasa, Superconducting Dome in a Gate-Tuned Band Insulator, *Science.* 338 (2012) 1193–1196.

[11] D. Costanzo, S. Jo, H. Berger, A.F. Morpurgo, Gate-induced Superconductivity in atomically thin MoS_2 crystals, *ArXiv*151203222 Cond-Mat. (2015).

[12] W. Shi, J. Ye, Y. Zhang, R. Suzuki, M. Yoshida, J. Miyazaki, N. Inoue, Y. Saito, Y. Iwasa, Superconductivity Series in Transition Metal Dichalcogenides by Ionic Gating, *Sci. Rep.* 5 (2015) 12534.

[13] S. Jo, D. Costanzo, H. Berger, A.F. Morpurgo, Electrostatically Induced Superconductivity at the Surface of WS_2, *Nano Lett.* 15 (2015) 1197–1202.

[14] J.M. Lu, O. Zheliuk, I. Leermakers, N.F.Q. Yuan, U. Zeitler, K.T. Law, J.T. Ye, Evidence for two-dimensional Ising superconductivity in gated MoS_2, *Science.* (2015) aab2277.

[15] Y. Saito, Y. Nakamura, M.S. Bahramy, Y. Kohama, J. Ye, Y. Kasahara, Y. Nakagawa, M. Onga, M. Tokunaga, T. Nojima, Y. Yanase, Y. Iwasa, Superconductivity protected by spin-valley locking in ion-gated MoS_2, *Nat. Phys.* 12 (2016) 144–149.

[16] X. Xi, Z. Wang, W. Zhao, J.-H. Park, K.T. Law, H. Berger, L. Forró, J. Shan, K.F. Mak, Ising pairing in superconducting $NbSe_2$ atomic layers, *Nat. Phys.* 12 (2016) 139–143.

[17] K.S. Novoselov, A.K. Geim, S.V. Morozov, D. Jiang, Y. Zhang, S.V. Dubonos, I.V. Grigorieva, A.A. Firsov, Electric Field Effect in Atomically Thin Carbon Films, *Science.* 306 (2004) 666–669.

[18] L. Wang, I. Meric, P.Y. Huang, Q. Gao, Y. Gao, H. Tran, T. Taniguchi, K. Watanabe, L.M. Campos, D.A. Muller, J. Guo, P. Kim, J. Hone, K.L. Shepard, C.R. Dean, One-Dimensional Electrical Contact to a Two-Dimensional Material, *Science.* 342 (2013) 614–617.

[19] P.J. Zomer, M.H.D. Guimarães, J.C. Brant, N. Tombros, B.J. van Wees, Fast pick up technique for high quality heterostructures of bilayer graphene and hexagonal boron nitride, *Appl. Phys. Lett.* 105 (2014) 13101.

[20] X. Chen, Z. Wu, S. Xu, L. Wang, R. Huang, Y. Han, W. Ye, W. Xiong, T. Han, G. Long, Y. Wang, Y. He, Y. Cai, P. Sheng, N. Wang, Probing the electron states and metal-insulator transition mechanisms in molybdenum disulphide vertical heterostructures, *Nat. Commun.* 6 (2015) 6088.

[21] K. Ueno, S. Nakamura, H. Shimotani, A. Ohtomo, N. Kimura, T. Nojima, H. Aoki, Y. Iwasa, M. Kawasaki, Electric-field-induced superconductivity in an insulator, *Nat. Mater.* 7 (2008) 855–858.

[22] J.T. Ye, S. Inoue, K. Kobayashi, Y. Kasahara, H.T. Yuan, H. Shimotani, Y. Iwasa, Liquid-gated interface superconductivity on an atomically flat film, *Nat. Mater. 9* (2010) 125–128.

[23] M.A. Khan, A. Bhattarai, J.N. Kuznia, D.T. Olson, High electron mobility transistor based on a GaN - $Al_xGa_{1-x}N$ heterojunction, *Appl. Phys. Lett.* 63 (1993) 1214–1215.

[24] R. Roldán, E. Cappelluti, F. Guinea, Interactions and superconductivity in heavily doped MoS_2, *Phys. Rev. B.* 88 (2013) 54515.

[25] T. Eknapakul, P.D.C. King, M. Asakawa, P. Buaphet, R.-H. He, S.-K. Mo, H. Takagi, K.M. Shen, F. Baumberger, T. Sasagawa, S. Jungthawan, W. Meevasana, Electronic Structure of a Quasi-Freestanding MoS_2 Monolayer, *Nano Lett.* 14 (2014) 1312–1316.

[26] C. Lee, H. Yan, L.E. Brus, T.F. Heinz, J. Hone, S. Ryu, Anomalous Lattice Vibrations of Single- and Few-Layer MoS_2, *ACS Nano.* 4 (2010) 2695–2700.

[27] J. Chang, L.F. Register, S.K. Banerjee, Ballistic performance comparison of monolayer transition metal dichalcogenide MX_2 (M = Mo, W; X = S, Se, Te) metal-oxide-semiconductor field effect transistors, *J. Appl. Phys.* 115 (2014) 84506.

[28] T. Ando, A.B. Fowler, F. Stern, Electronic properties of two-dimensional systems, *Rev. Mod. Phys.* 54 (1982) 437–672.

[29] Y.Z. Chen, N. Bovet, F. Trier, D.V. Christensen, F.M. Qu, N.H. Andersen, T. Kasama, W. Zhang, R. Giraud, J. Dufouleur, T.S. Jespersen, J.R. Sun, A. Smith, J. Nygård, L. Lu, B. Büchner, B.G. Shen, S. Linderoth, N. Pryds, A high-mobility two-dimensional electron gas at the spinel/perovskite interface of γ-$Al_2O_3/SrTiO_3$, *Nat. Commun.* 4 (2013) 1371.

[30] G.-B. Liu, W.-Y. Shan, Y. Yao, W. Yao, D. Xiao, Three-band tight-binding model for monolayers of group-VIB transition metal dichalcogenides, *Phys. Rev. B.* 88 (2013) 85433.

[31] D. MacNeill, C. Heikes, K.F. Mak, Z. Anderson, A. Kormányos, V. Zólyomi, J. Park, D.C. Ralph, Breaking of Valley Degeneracy by Magnetic Field in Monolayer $MoSe_2$, *Phys. Rev. Lett.* 114 (2015) 37401.